Electrochemical Science Advances

Chemistry Europe
European Chemical Societies Publishing

RESEARCH ARTICLE OPEN ACCESS

NMR Methods for the Evaluation of Separation Mechanisms Utilised for the Recycling of PFSA Ionomer Membranes

Robert Rameker[1,2] | Sven Jovanovic[1] | Maik Plüm[3] | André Karl[1] | Eva Jodat[1] | Günter Schmid[3] | Rüdiger-A. Eichel[1,4,5] | Josef Granwehr[1,2]

[1]Institute of Energy Technologies, Fundamental Electrochemistry (IET-1), Forschungszentrum Jülich, Jülich, Germany | [2]Institute of Technical and Macromolecular Chemistry, RWTH Aachen University, Aachen, Germany | [3]Siemens Energy Global GmbH & Co. KG, München, Germany | [4]Institute of Physical Chemistry, RWTH Aachen University, Aachen, Germany | [5]Faculty of Mechanical Engineering, RWTH Aachen University, Aachen, Germany

Correspondence: Sven Jovanovic (s.jovanovic@fz-juelich.de)

Received: 4 August 2025 | **Revised:** 13 March 2026 | **Accepted:** 23 March 2026

Keywords: catalyst layer separation | low vs. high-field NMR | nuclear magnetic resonance spectroscopy | perfluorosulfonic acid ionomer membranes | proton exchange membrane recycling

ABSTRACT

Proton exchange membrane (PEM) electrolysis is considered a promising technique for producing green hydrogen at high purity, yet it has not been implemented industrially on a large scale. To make this technology economically feasible, the industry is in search of ways to recycle the membranes and the catalyst material. A particular benefit of membrane recycling is that it can prevent high financial penalties, as a ban on the production of PFAS materials is currently under discussion. One suggested recycling process is based on the use of alcohol to separate the catalyst material from the PEM. However, the influence of the separation mechanism on the structure of the PEM is often disregarded. In this work, ^{19}F solid-state NMR techniques as well as ^{1}H diffusion NMR were applied to analyse the invasiveness of such a separation technique on a short-side chain perfluorosulfonic acid (ssc-PFSA) ionomer, which is a widely used PEM material for high-durability electrolysis cells. Therefore, a sample preparation routine was established to mimic relevant states in the conditioning and recycling process of PEM materials. Based on the evolution of ^{19}F spectra, it was found that a water-isopropanol mixture causes changes in the chemical composition of the polymer structure. In conjunction with signal analysis, various degradation pathways are discussed that are initiated by ultrasound during electrode separation. Relaxation experiments also suggest that the polymer morphology is significantly altered during the entire production process, and particularly during the separation process.

1 | Introduction

The stark impact of rising CO_2 emissions and associated global warming has underscored the urgency of developing climate-neutral alternatives to fossil fuels [1]. However, an additional challenge is to meet an ever-increasing global hydrogen demand. In this context and to advance environmentally sustainable technologies, the proton exchange membrane water electrolysis (PEMWE) offers a viable way to transform and store energy through the production of 'green' hydrogen [2, 3]. In addition, there is a high demand for hydrogen, as part of so-called power-to-X systems that produce platform chemicals, which can only be covered by efficient and sustainable hydrogen production [4, 5]. As PEM technology has been thoroughly researched and can be operated at high energy efficiency [6, 7], this method is about to be implemented on a large scale in the chemical industry soon

Robert Rameker is the first author of this work

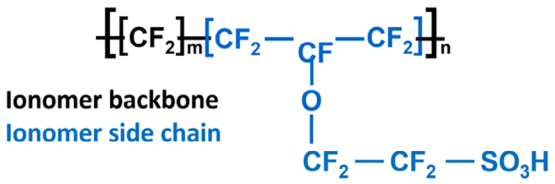

FIGURE 1 | Sketch of the chemical structure of an SSC-PFSA ionomer unit with marking of the backbone and side chain.

[4]. But at present, only 4% of global hydrogen demand is covered by 'green' hydrogen, which is produced by water electrolysis using electricity from renewable energy sources, while the largest share is still produced from fossil fuels [8]. Even though the PEMWE technology is distinguished by such advantages as high current densities, high voltage efficiency, fast system response, compact design and the high purity of the product gases, it is hampered by some specific disadvantages. These drawbacks are the high cost of the components, limited reserves of the state-of-the-art catalyst materials, acid corrosion and the vulnerability of the whole system in general and the PEM in particular to the full range of degradation mechanisms in both operation modes [9, 10]. An additional, very critical issue is the danger arising from polyfluoroalkyl substances (PFAS), which are the basic substances of the most commonly used PEM materials. For this reason, a ban on polyfluoroalkyl substances (PFAS) is being discussed, which would force energy companies to use these PEM materials thriftily to prevent high financial penalties. In June 2023, for example, the companies 3M, Chemours, DuPont and Corteva have been sentenced to a total of 11 billion US dollars for contamination of drinking water with PFAS chemicals [11, 12]. Human consumption of inert PFAS chemicals through drinking water is linked to health problems such as liver damage, thyroid disease, fertility problems and cancer [13, 14]. As long as no PFAS-free PEM material has been developed that could compete with PFAS-based PEM materials in terms of proton conductivity and selectivity, membrane recycling could be a suitable way to reduce the waste of PFAS substances significantly. In their status report on water electrolysis and hydrogen in the European Union, 2024, the Joint Research Centre of the European Commission stated that support should be granted for research and development of innovative recycling methods for hydrogen electrolyser components, offering secondary materials of high quality [15]. While great progress has been made on recycling of lithium-ion batteries [16–20], photovoltaics [20–22] and wind turbines [20], the possibilities of recycling PEMs have not yet been investigated in depth [22].

PEMs usually are made of perfluorinated sulfonic acid (PFSA) ionomers, which consist of a backbone of -CF_2- units and side chains with sulfonic acid groups at their end (see figure 1). Depending on the length of the side chain, the terms short side chain (ssc) and long side chain (lsc) are often used in literature [23]. In general, desirable PEM materials are characterised by high inertness and high proton diffusivity. While chemical inertness, which is enabled by perfluorination of the backbone and side chain-carbons, should enable a long lifetime of the PEM, the formation of micro-channels should enable a high diffusivity of protons. In the humid state, the ionomer forms a water-bearing channel-like spatial structure, with the side chains reaching into the channels and ensuring selective diffusion of the protons [24]. A high proton transport in combination with a high proton selectivity is provided by the sulfonate groups present on the side chains, which facilitate proton diffusion.

PEM degradation can be subdivided into reversible and irreversible degradation [25]. Reversible degradation is caused especially by parasitic foreign ions such as Fe^{3+} or Al^{3+}, which reduce the performance of the membrane but can be removed by H_2SO_4 treatment [26–28]. Meanwhile, irreversible degradation mechanisms include mechanical and thermal degradation mechanisms such as membrane thinning [29], pinhole or crack formation [30], and the formation of hot spots and local membrane swelling caused by an uneven current distribution [25]. Moreover, PEMs are eventually prone to chemical degradation, which causes membrane thinning and release of F^- ions by radical attack [31]. Radical-initiated reactions are usually outlined as origins of these chemical degradation mechanisms, whereby the radicals attack both the backbone as well as the polar side chains of the PEM polymer [32, 33]. All these degradation phenomena are the reason why PEM water electrolysis is still affected by severe limitations today, which hamper economic operation.

To effectively commercialise PEMWE technology, material costs have to be reduced, and ionomers that offer a longer PEM lifetime with the same selectivity and proton exchange efficiency need to be developed [34]. One way to save material costs is to separate the PEM from the catalyst layers and to recycle both components [35]. Different recycling approaches have been reported. Many of these include the use of a mixture of water and small alkyl alcohols such as isopropanol [36, 37]. The primary aim of these methods was to recycle the expensive catalyst layer materials. Nevertheless, it is considered desirable to recycle the PEM as well, as it is also made of a high-value perfluorinated ionomer material. An approach to recycle both the catalyst material and the PEM was reported by Moghaddam et al. [38], where the PEM has been completely dissolved in acidic or basic solutions and recast in three different ways. The results of the analytical methods have shown that a recycled Nafion membrane had the same characteristics concerning proton conductivity as a recast Nafion membrane from a pristine commercial Nafion membrane. It must still be noted that a recast Nafion membrane can have different structural properties than a pristine commercial membrane. However, the recycling process may be too complex for large-scale industrial implementation. Furthermore, solvating and recasting the PEM is solvent and energy-intensive. Therefore, methods for separating the catalyst layers from the PEM without the need to dissolve the PEM are considered preferable for industrial applications. Recycling processes in which the device is separated directly into its components with minimal solvent and energy consumption are also found in the form of direct recycling of lithium-ion batteries, which is proposed as a viable alternative to conventional recycling [39, 40].

In a recent publication, the PEM material is separated from the catalyst layers by the use of organic solvents and ultrasound [41]. While the effectiveness of this separation method is proven by different imaging techniques, NMR spectroscopy could offer a set of methods to check whether the separation technique is also non-invasive on the chemical structure and morphological properties of the ionomer material on the molecular scale.

NMR spectroscopy is a well-established method for the investigation of PEMs due to the wide range of chemical and structural information the method can provide. A large number of NMR techniques for the analysis of chemical and structural properties of PEMs have been reported [32, 42–48]. To determine the molecular structure and mobility changes within the ionomers' functional groups, solid-state ^{19}F NMR has been applied using the magic-angle spinning (MAS) technique [49, 50]. Thereby, the change in the relative signal ratios between the different resonances can be observed to study whether degradation preferably took place in the polymer backbone or the side chain [42, 43]. The longitudinal relaxation time (T_1) [32, 45] allows changes in the correlation time of functional groups to be monitored, which are linked to structure and mobility, and therefore the properties of the PEM polymer. In addition to the ^{19}F MAS studies using a high-field spectrometer, ^{1}H experiments on an 80 MHz low-field spectrometer were performed, where proton mobility was examined by pulsed-field-gradient (PFG) and T_2 relaxation studies. Ion diffusion behaviour in particular plays a key role when it comes to evaluating the suitability of a membrane material for water electrolysis or fuel cell operation [51–53]. By means of ^{1}H NMR, previous works have demonstrated the existence of different water domains within the individual pores in Nafion membranes as a function of the water uptake and conditioning [54, 55, 45, 56]. The intent of the manuscript is not to present an industrially applicable recycling method that is both minimally invasive and saves resources and energy. Rather, it demonstrates the significance of different NMR methods, which are partially suitable for industrial quality control, based on a recycling method that is still in need of optimisation. Thus, ^{19}F studies of polymer structure can be correlated to ^{1}H studies of proton transport, establishing a structure-property analysis of the PEM material, and bridging the link between high-field NMR in academia and benchtop NMR in an industrial context.

2 | Experimental Methods

2.1 | Setup

Figure 2 illustrates the fabrication procedure of the samples investigated in this study. The dry pristine PEM (DP-PEM) has been analysed as received. To ensure complete hydration, the hydrated pristine PEM (HP-PEM) was immersed in deionised water for 24 h. The hydrated separated PEM (HS-PEM) was analysed to understand the effect of the catalytic-layer separation method on the membrane, unbiased by the influence of the catalytic layer itself. Therefore, the separation method was applied to the surface of an HP-PEM in the following way: After hydration, the HP-PEM was placed on a plastic block. Then, a few drops of isopropanol (2-propanol, >99.5%, Carl Roth) were dropped onto an ultrasonic toothbrush, and the cathode side was brushed for 1 min. Residues of the catalytic material were removed from the PEM surface with a clean paper tissue and deionised water. The ultrasonic toothbrush was cleaned with water and again drizzled with a few drops of isopropanol. This procedure was repeated two more times, so that in total, the surface was brushed for 3 min. The same procedure was performed for the anode side after exchanging the toothbrush head. Even though no catalyst layers had yet to be separated, the separation process was performed on the HP-PEM to study the influence of the separation process itself on the PEM chemistry and morphology, independent of catalyst particles. The light blue layers in Figure 2 are intended to clarify that although the separation step was carried out, no catalyst was removed. On the DP-MEA, the separation process was performed to prevent the catalyst layers from influencing the magnetic field during the measurements and, therefore, the resulting spectrum. After hydration of the DP-MEA at the same conditions as for the DP-PEM, the catalyst layers were removed with the same procedure that was applied to the HP-PEM to produce the HS-MEA. Here, each side of the MEA was brushed six times, so that in total, both sides of the MEA were brushed for 6 min. The HHS-MEA was produced by heating the DP-MEA to 60°C for 5 h in deionised water and performing the separation procedure as for the HS-MEA.

2.2 | Sample Preparation for ^{19}F Solid-State NMR Experiments

7x7 mm samples were stored in deionised water until use. For MAS NMR sample preparation, the samples were dabbed with a precision paper wipe to remove surface water and cut into strips 0.2–0.5 mm in width with ceramic scissors. The strips were filled into Bruker (Ettlingen, Germany) 1.3 mm ZrO_2 MAS rotors. To achieve constant hydration for the hydrated samples, the unsealed rotors were packed into a glove bag together with the 1.3 mm SP_1 drive caps and stored in an Espec SH-242 humidity chamber for at least 72 h to equilibrate at 25°C and 95% relative humidity. After equilibration, the glove bag was taken out of the climate chamber and closed immediately to conserve the atmosphere of the climate chamber. Then the rotors were sealed with a 1.3 mm SP_1 drive cap inside a glove bag at the conditions of the climate chamber.

2.3 | Sample Preparation for ^{1}H Diffusion NMR Experiments

40 × 20 mm samples were stored in deionised water until use. The samples were cut into 0.15–0.25 mm wide strips and packed into air-tight screw-top 5 mm NMR tubes. To achieve a constant PEM hydration, the unsealed NMR tubes and the screw top caps were packed into a glove bag and stored in an Espec SH-242 (Hudsonville, Michigan, USA) climate chamber at 25°C and 95% relative humidity for at least 7 days. After equilibration, the glove bag was taken out of the climate chamber and closed immediately to conserve the atmosphere of the climate chamber. Afterwards, the NMR tubes were sealed inside the closed glove bag.

2.4 | ^{19}F NMR Experiments

High resolution ^{19}F NMR spectra were recorded on a Bruker Avance Neo spectrometer using a Bruker Ascend Aeon 800WB (18.8 T, 800 MHz for ^{1}H) magnet and a PH MASDVT800W2 BL1.3 N-P/F-H 1.3 mm MAS probe. The temperature was set to 25°C, and the MAS spinning frequency was 40 kHz.

The ^{19}F centre frequency was set to match the $(CF_2)_n$ signal at −121 ppm, with a sweep width of 199.213 ppm. The recycle delay

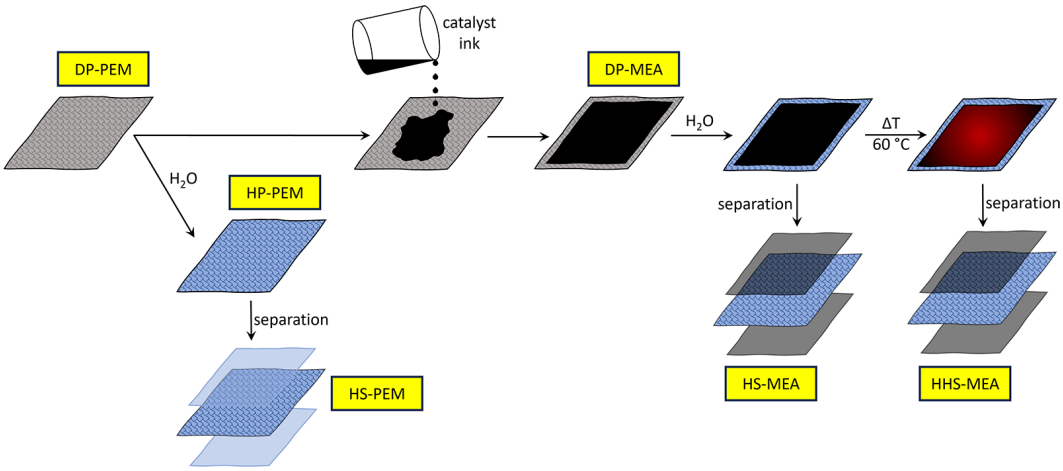

FIGURE 2 | Scheme of the fabrication steps to manufacture a begin-of-live MEA for PEM electrolysis from a pristine PEM. The labels in yellow boxes refer to samples investigated by NMR. A dry, pristine PEM (DP-PEM) was hydrated and thus converted into a hydrated, pristine PEM (HP-PEM). By applying the separation technique as a test on the HP-PEM, it was converted into a hydrated, separated PEM (HS-PEM). By the addition of the catalyst layers, the DP-PEM was converted into a dry, pristine MEA (DP-MEA). By hydration and application of the separation technique to the DP-MEA, a hydrated, separated MEA (HS-MEA) was formed. By heating the MEA at 60°C for 5 h and application of the separation technique, a hydrated, heated, separated MEA (HHS-MEA) was formed.

was set to a value between 1 and 10 s, depending on the T_1 relaxation time of the corresponding sample. The 90° pulse power was set to 45 W, and the 90° pulse length was determined to lie between 2.3 and 2.6 µs, depending on the sample.

The raw data were processed using a custom Python script (Python version 3.9) (see Supporting Information). Fitting was performed using Lmfit (version 1.2.2) [57]. The resulting spectra were fitted using Pseudo–Voigt functions providing the integral, the centre frequency, the full width at half maximum and the Pseudo–Voigt fraction. The OCF_2 signal and the CF_b signal were fitted using a single Pseudo–Voigt profile. The $(CF_2)_n$ signal was fitted using three pseudo-Voigt profiles and one Lorentzian profile with centre frequencies fixed between −120 and −123 ppm. The SCF_2/CCF_2 signal was fitted using one or two pseudo-Voigt profiles depending on the shape of the signal with its centre frequencie(s) constrained between −116 and −118 ppm.

The intensities of the SCF_2/CCF_2 signal, the OCF_2 signal and the CF_b signal with respect to the $(CF_2)_n$ signal were calculated from the fit components and normalised to the $(CF_2)_n$ signal integral, that is, the sum of the $(CF_2)_n$ signal components. The error was calculated using Gaussian error propagation. For this purpose, the average noise per 1 ppm was determined using the range between −100 ppm and −90 ppm. Using Equation (1),

$$n_{\text{signal}} = 4\,\sigma\,n_{\text{ppm}}, \tag{1}$$

the noise of each signal was calculated with σ being the half-width at half maximum of a signal and n_{ppm} being the noise per ppm. Using the method of Gaussian error propagation, the calculated relative error for each sample was in a range between 1% for the SCF_2/CCF_2 signal and 10% for the CF_b signal.

The T_1 relaxation time experiments were recorded on a Bruker Avance III HD spectrometer using a Bruker Ascend 400WB (9.6 T, 400 MHz for ^{1}H) Magnet and a PH MASDVT 400W1 BL1.3 N-P/H NO-I/E probe. The temperature was set to 25°C, and the MAS spinning frequency was set to 30 kHz. The 90° pulse power was set to 25 W, and the 90° pulse length was set to 1.1 to 1.3 µs, depending on the maximum of the parameter optimisation experiment.

The T_1 relaxation time constant was determined using a saturation recovery pulse sequence with logarithmically spaced delays between 0.008 and 7.5 s. The number of pulses during the saturation pulse train was 256, and the delay between the pulses was 0.5 ms.

The data was analysed by displaying the integrals of the different resonances against the variable delay and regressed by an exponential fit to determine T_1 (Equation 2):

$$M_z = M_0 \cdot \left(1 - e^{-\frac{t}{T_1}}\right). \tag{2}$$

The error of T_1 was calculated from the deviation of the exponential fit from the deviation of the integral values from the exponential fit.

2.5 | ^{1}H Pfg Nmr

The proton diffusion experiments were recorded on a Spinsolve MultiX ^{13}C 80 MHz spectrometer. The temperature was set to 26°C.

The proton diffusion coefficient was determined using a pulsed gradient stimulated echo (PGSTE) sequence with constant gradient duration, constant diffusion time and variable gradient strength. A total of 16 different gradient strength values were set. The maximum gradient strength g was 0.528 T m^{-1}, the minimum gradient strength 0.0605 T m^{-1}. The gradient duration δ was 0.0051 s, and the diffusion time Δ was 0.02 s.

The signal intensity during the PGSTE experiment can be described by the Stejskal–Tanner equation (Equation 3) [58]:

$$\frac{S}{S_0} = exp\left\{-\gamma^2 g^2 \delta^2 \left(\Delta - \frac{1}{3}\delta\right) D\right\}. \quad (3)$$

According to Le Bihan, the Stejskal–Tanner equation is abbreviated by introducing the b factor (Equation 4) [59, 60]:

$$\frac{S}{S_0} = exp\{-bD\}. \quad (4)$$

The b factor includes the g, Δ, δ variables and the gyromagnetic ratio γ. Using an exponential fit, the self-diffusion coefficient D could be determined.

2.6 | Ion Exchange Capacity Analysis

The ion exchange capacity was calculated from the intensity of the OCF_2 signal, which can be assigned to the side chain, in relation to the sum of the SCF_2/CCF_2 signal and the $(CF_2)_n$ signal, which are assigned to the backbone according to Moukheiber et al. [44]. This results in the quotient of the backbone and side chain signal R (Equation 5):

$$R = \frac{I_{OCF_2}}{I_{(CF_2)_n} + I_{SCF_2/CCF_2}}. \quad (5)$$

The upper error R^+ and the lower error R^- were calculated based on the errors of the signal ratios (Equations 6a and 6b):

$$\Delta_{R^+} = \frac{I_{OCF_2} - \Delta_{I_{OCF_2}}}{I_{(CF_2)_n} + I_{SCF_2/CCF_2} + \Delta_{I_{SCF_2/CCF_2}}} \quad (6a)$$

$$\Delta_{R^-} = \frac{I_{OCF_2} + \Delta_{I_{OCF_2}}}{I_{(CF_2)_n} + I_{SCF_2/CCF_2} - \Delta_{I_{SCF_2/CCF_2}}} \quad (6b)$$

From the ratio R, the number of tetrafluoroethylene units was calculated (Equation 7):

$$n = \frac{1}{2R} - 1. \quad (7)$$

With the molecular weight of a short side chain unit being M_{ssc} = 278 g mol^{-1} and the molecular weight of each C_2F_4 unit being 100 g mol^{-1}, the equivalent weight of the ionomer with respect to the sulfonic acid groups was calculated (Equation 8):

$$EW = M_{ssc} + n \cdot M_{C_2F_4}. \quad (8)$$

The calculated equivalent weight of the DP-PEM was 718 g mol^{-1}, which is in good agreement with the equivalent weight of commercially available ssc-PFSA ionomer membranes [44]. The ion exchange capacity IEC was calculated as Equation (9):

$$IEC = \frac{1000}{EW}. \quad (9)$$

In this work, the ion exchange capacity was calculated from ^{19}F spectra according to a method published by Moukheiber et al. In this method, the ratio of the side chain signal and the backbone signal was calculated by dividing the intensity of the OCF_2 signal, which is attributed to the ionomer side chain, by the intensity of the combined $(CF_2)_n/SCF_2/CCF_2$ signals, which are attributed to the ionomer backbone [44].

3 | Results

The ^{19}F NMR spectrum of the DP-PEM is shown in Figure 3a. It was fitted with the OCF_2 signal at −78 ppm, the SCF_2/CCF_2 signal at −117 ppm, the $(CF_2)_n$ signals at −122 ppm, and the CF_b signal at −138 ppm. In literature, corresponding signals with comparable intensity ratios were detected in measurements on short-side chain perfluorosulfonic acid ionomer proton exchange membranes (ssc-PFSA ionomer PEMs) [42, 46]. The spinning sideband of the OCF_2 signal at −131 ppm must be taken into account here.

By fitting the $(CF_2)_n$ signal using four components instead of one, the residuals could be reduced from 2%–5% to below 1% [32]. Even if the $(CF_2)_n$ group is considered as a single functional group, the chemical shift of individual CF_2 units may still experience a distribution of chemical shifts. For this reason, the signal of the CF_2 groups next to the CF_b branching point (here: CCF_2 groups) has a similar chemical shift as the signal of the SCF_2 group.

The ^{19}F NMR spectrum of the HP-PEM is depicted in Figure 3b. The chemical shift of the signals does not change compared with the DP-PEM, but the shape of specific signals changes. For the HP-PEM, the linewidths of the side chain and branching point signals are significantly lower compared with the DP-PEM. Nevertheless, a single pseudo-Voigt profile was still sufficient for the regression of the SCF_2/CCF_2 signal. Also, the $(CF_2)_n$ signal is slightly narrower compared with Figure 3a. This finding indicates that the T_2^* relaxation time, which according to Equation (10),

$$\Delta_{1/2} = \frac{1}{\pi \cdot T_2^*}, \quad (10)$$

is inversely proportional to the full line width at half maximum $\Delta_{1/2}$, is increased by the hydration process, indicating an increased mobility of the respective functional groups.

In Figure 3c, the spectrum of the HS-PEM is shown. It consists of the same signals as the spectra of the pristine and the hydrated PEM. The OCF_2 signal and especially the SCF_2/CCF_2 signal appear even narrower than in the spectrum of the HP-PEM (Figure 3b), and in the case of the SCF_2/CCF_2 signal, a regression with only one pseudo-Voigt profile was not sufficient anymore. Since the signal has a recognisably different shape with a significantly sharper tip, an additional pseudo-Voigt profile of low intensity and line width is required for optimal regression.

Figure 3d depicts the spectrum of the DP-MEA. A combination of two pseudo-Voigt profiles was not necessary anymore to get a sufficient fit due to the broader shape of the SCF_2/CCF_2 signal.

The spectrum of the HS-MEA is shown in Figure 3e. As for the spectrum of the HS-PEM, an additional pseudo-Voigt profile

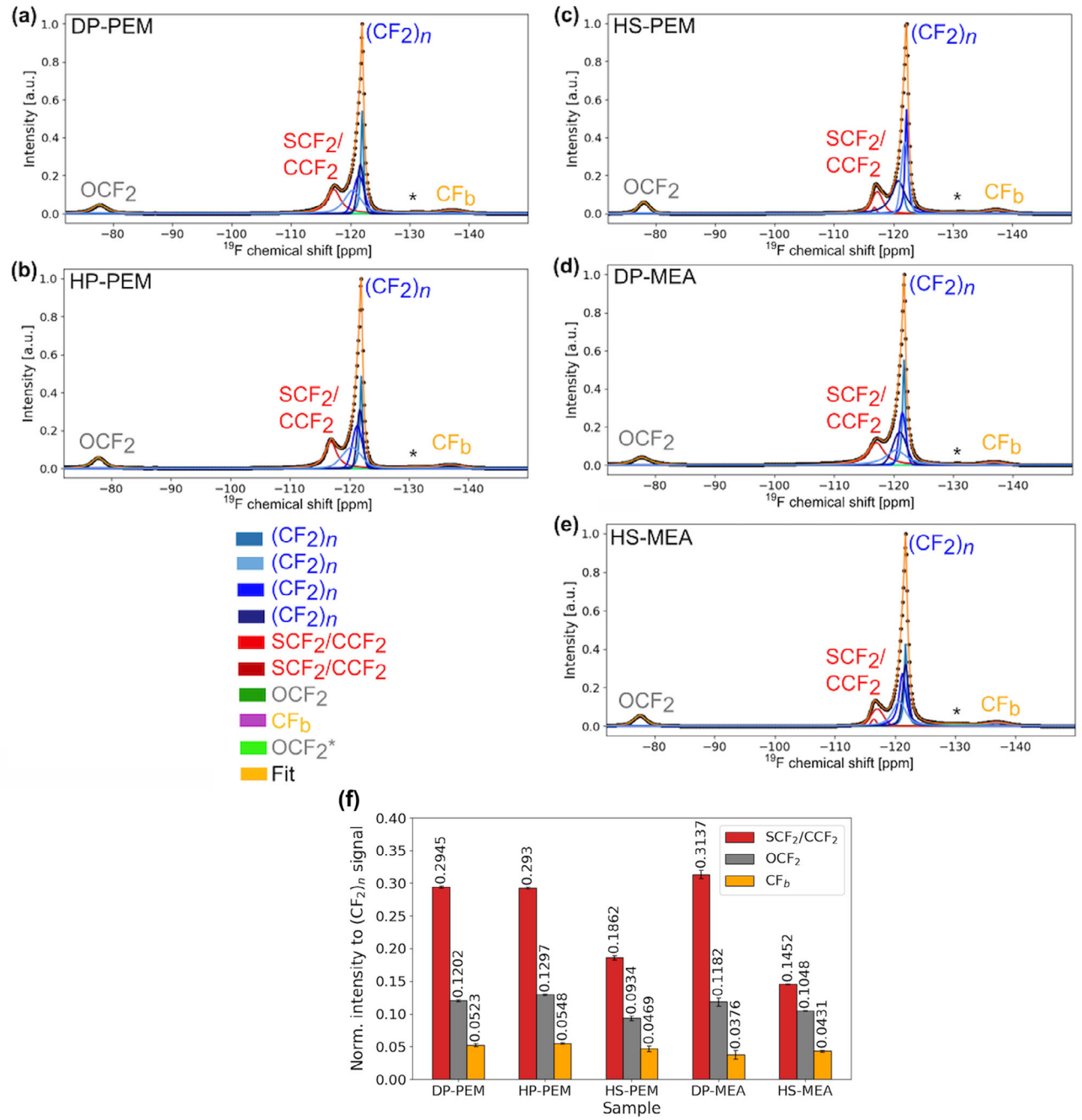

FIGURE 3 | One-dimensional ^{19}F NMR spectrum of **(a)** the DP-PEM, **(b)** the HP-PEM, **(c)** the HS-PEM, **(d)** the DP-MEA and **(e)** the HS-MEA, recorded at a MAS spinning frequency of 40 kHz. Experimental data are indicated by black dots; the resulting fit is displayed by the orange line, and the Lorentzian and pseudo-Voigt functions are illustrated in the colours given in the legend. The asterisks (*) indicate the spinning sideband of the OCF_2 signal. A zoom-in figure of this feature is provided in the Supporting Information. Relative intensities of the SCF_2/CCF_2 (red), the OCF_2 (grey), and the CF_b (orange) signal are displayed in **(f)**. The intensities of the signals of the ^{19}F spectra were determined using the integrals given by the pseudo-Voigt regression. The intensities of the signals were normalised to the sum of integrals of the $(CF_2)_n$ signal.

between −116 and −118 ppm was necessary for an optimal regression of the data points. In general, the spectrum was very similar to that of the HS-PEM in terms of signal shapes and intensities. The spectrum of the HHS-MEA, which does not contain any additional features, is available in the Supporting Information Material.

Concerning the HP-PEM, HS-PEM and HS-MEA, it is also observed that the SCF_2/CCF_2 signal is clearly separated from the $(CF_2)_n$ signal. In contrast to the hydrated samples, the SCF_2/CCF_2 signal of the DP-PEM and DP-MEA is broader and overlaps with the $(CF_2)_n$ signal to a greater extent.

In Figure 3f, the calculated relative intensities of the SCF_2/CCF_2 signal, the OCF_2 signal and the CF_b signal with respect to the $(CF_2)_n$ signal are displayed. The calculated relative intensity of the SCF_2/CCF_2 signal for the DP-PEM and HP-PEM is in good agreement with each other and with the chemical structure of

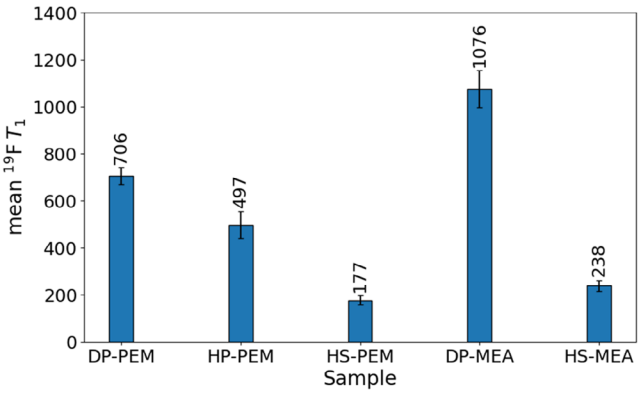

FIGURE 4 | Averaged T_1 relaxation time values for the $(CF_2)_n$, SCF_2/CCF_2, OCF_2 and CF_b signal from the ionomer structure. T_1 was determined using a saturation recovery experiment and a single-exponential fit of the signal integrals vs. the variable delay.

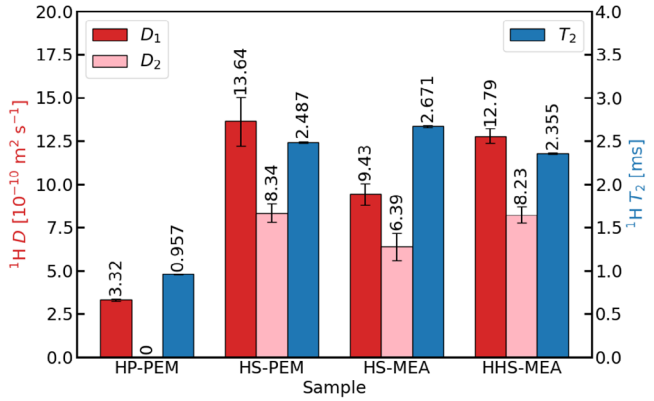

FIGURE 5 | ^{1}H diffusion coefficients D and T_2 relaxation time constants of the water-containing samples. The signal intensity values of the hydrated PEM (sample 2) vs. gradient strength showed the best agreement with a single-exponential fit, while the data points of the other samples showed a better agreement with a double-exponential fit, suggesting two different diffusion mechanisms.

an ssc-PFSA ionomer with an equivalent weight of 720 g mol^{-1}. The deviation of approx. 8% between the relative intensity of the SCF_2/CCF_2 signal of the DP-PEM and HP-PEM can be attributed more to the complexity of the fit model with regard to the overlapping SCF_2/CCF_2 and $(CF_2)_n$ signals than to an actual degradation of OCF_2 groups. A common ssc-PFSA ionomer with an equivalent weight of 720 g mol^{-1} possesses a short side chain and 8.8 units of CF_2 per side chain [44]. As the relative intensities of the OCF_2 signal and the CF_b signal are roughly similar for the DP-PEM and the HP-PEM, no chemical alteration is indicated here.

For the HS-PEM, a decrease of the relative SCF_2/CCF_2 signal by 40% compared with the HP-PEM is observed. The relative OCF_2 signal decreased by 28%.

The signal ratios of the DP-MEA are in good agreement with the pristine PEM and the hydrated PEM concerning the relative intensities of the SCF_2/CCF_2 signal and the OCF_2 signal. However, the relative CF_b signal of the DP-MEA is significantly lower compared with the pristine and the hydrated PEM.

The relative intensities of the SCF_2/CCF_2 and OCF_2 signals of the HS-MEA are significantly lower in comparison to the DP-MEA. Compared with the HS-PEM, the relative SCF_2/CCF_2 signal of the HS-MEA is slightly lower, while the relative OCF_2 signal is slightly higher.

In Figure 4, the longitudinal relaxation times T_1 of all functional groups are shown. Since T_1 values for the single functional groups have been reported to be influenced by spin diffusion due to dipolar couplings within the ^{19}F network [32], the T_1 values of the different functional groups converge. Therefore, the average T_1 values provide an estimate of the mobility of the ionomer structure in each sample. Among the different samples, a decrease in the T_1 relaxation time was observed by the hydration of the membrane (HP-PEM), and a further decrease by the separation process (HS-PEM). This indicates that the relaxation time of the sample lies in the slow-motion regime relative to the maximum of the relaxation dispersion curve. The T_1 relaxation time of the DP-MEA was significantly higher than the T_1 of the DP-PEM. By the separation process on the DP-MEA, a decrease in T_1 was observed as well.

In Figure 5, the ^{1}H diffusion coefficients of the hydrated samples are shown. For the HP-PEM, only a single diffusion component was observed. In contrast, the separated samples HS-PEM, HS-MEA and HHS-MEA exhibited two diffusion components.

The diffusion coefficient of 3.32 $\times 10^{-10}$ m^2 s^{-1} determined for the HP-PEM was in good agreement with the diffusion coefficients obtained for high water uptake ratios of >10 water molecules per sulfonic acid group [54, 61]. A significant increase in proton diffusion was observed in the two diffusion coefficients of the HS-PEM. The diffusion coefficients of the HS-MEA, however, were slightly lower. By heating the sample up to 60°C during the following step of the fabrication process, the diffusion coefficients of the HHS-MEA recovered to the levels of the HS-PEM. The proton T_2 relaxation time was increased by a factor of 2–3 for the separated samples compared with the HP-PEM.

4 | Discussion

The signal ratios outlined in Figure 5 indicate chemical degradation of the respective functional groups. A decrease in the ratio indicates a partial chemical degradation of a functional group from the molecular ionomer structure [43]. The decrease of the SCF_2/CCF_2 signal of the HS-PEM compared with the HP-PEM may indicate a degradation of sulfonic acid groups. The extent to which sulfonic acid groups and complete side chains were abstracted from the ionomer structure by the separation mechanism was calculated from the signal ratios. The calculation given in the Supporting Information material relates exclusively to the influence of the separation mechanism, i.e. the HP-PEM and HS-PEM samples. Here, it must be considered that the chemical environment of two of the CCF_2 fluorine nuclei is significantly changed, and thus the chemical shift is likely to shift back to the frequency of the $(CF_2)_n$ signal. Taking this into consideration, the relative degradation rates depicted in Figure 6

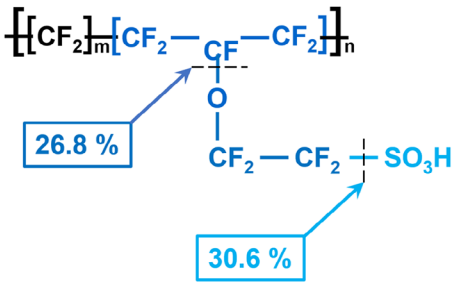

FIGURE 6 | Calculated relative degradation rate of the sulfonic acid groups and O-CF_2-CF_2 fragments induced by the separation mechanism based on the changed relative signal intensities.

were calculated. The relative loss of sulfonic acid groups by the separation mechanism is 30.6%. The relative loss of sulfonic acid groups is 26.8%, so that 3.8% of sulfonic acid groups were separated without scission of the corresponding side chain. As this calculation is based solely on the relative signal intensities and the degradation of the backbone has been neglected here, this can only be regarded as an approximation. At this point, it is unclear if the degradation of the sulfonic acid groups and complete side-chain fragments depend on each other or not.

The process of catalyst separation by ultrasonication in a mixture of isopropanol and water seems to potentially induce a variety of degradation mechanisms, as suggested by the altered signal ratios. It is reported that ultrasound, considered a mild source of energy, can mechanically generate hotspots of high energy in the material [62]. This induces changes in the spatial structure, as it is suggested based on the ^{19}F T_1 relaxation times. At the same time, ultrasound reduces the activation energy of the oxidation of isopropanol to acetone [63]. With acetone as a strong nucleophile, nucleophilic attacks on the SCF_2, OCF_2 and CF_b group are conceivable. Due to the static disorder induced by the ultrasound, there is also less of a steric hindrance to these reactions. At the same time, thermal breakage of the C–S bond by the ultrasound as an initiator of chemical degradation should still be considered, especially as the C–S bond possesses a lower mean binding energy of 272 kJ mol^{-1} compared with C–C (348 kJ mol^{-1}), C–O (358 kJ mol^{-1}) and C–F bonds (489 kJ mol^{-1}) [64]. This bond breakage could be the starting point in a radical degradation mechanism similar to the mechanism induced by the Fenton reaction [32]. As the SCF_2 group makes up only one-third of the SCF_2/CCF_2 signal, the significant decrease in the signal is also influenced by an alteration of the CCF_2 groups. An explanation may be that the signal of the CCF_2 group has a very similar chemical shift to $(CF_2)_n$ when the complete side chain has been degraded.

The observed decrease of the CF_b signal for the DP-MEA may be caused by a broadening of the pristine MEA CF_b signal due to the presence of the platinum catalyst and, therefore, an inaccurate fit as indicated by the error bar.

The comparison of the signal ratios of the HS-PEM and the HS-MEA indicates that the degradation mechanism during the separation process is influenced by the catalyst material: while the thermal degradation of the sulfonic acid group might be enhanced by the catalyst, the side chain scission by the isopropanol seems to be slightly inhibited by the catalyst layers. A possible explanation for this could be that the isopropanol is blocked by the catalyst layers before it is separated from the PEM. Therefore, a smaller amount of the isopropanol passes the catalyst layers and saturates the pure ionomer material. Thus, fewer isopropanol molecules are protonated due to the super-acidic conditions inside the PEM, inducing fewer side-chain cleavage reactions.

While the comparison of the signal ratios among the samples of the different fabrication steps reveals information about alteration concerning the molecular structure of the ionomer, relaxation times provide information about changes in the spatial structure of the ionomer and the mobility of the different functional groups due to water uptake. All functional groups possess similar ^{19}F T_1 values, suggesting an equilibration of relaxation times along the polymer chain due to strong spin diffusion. This is in line with the observations made by Ghassemzadeh et al., who found that the ^{19}F T_1 relaxation times of the individual functional groups in a lsc-PFSA ionomer do not deviate from each other within one sample [32]. Concerning T_1, a decrease was observed after hydrating the membrane, as an additional relaxation pathway is provided by the presence of water. This observation is even more evident regarding the hydrated, separated PEM. The decrease in T_1 could be associated with polymer backbone and side-chain motions becoming less restricted. During the separation process, the swelling in water of the membrane increased by 90% in the perpendicular direction to the plane. This suggests that even more water is absorbed by the membrane, and thus the relaxation of the signals via the water pathway becomes dominant. In the DP-PEM, chain motions in the ionomer are expected to be more restricted, as the channel-like water transport system has not yet formed.

One possible explanation for the swelling behaviour caused by the separation process is the addition of isopropanol. While water is a polar molecule, which therefore only interacts with the functional groups of the side chain and, for that reason, is responsible for the formation of the pore structure, isopropanol also has a hydrophobic component. Isopropanol, therefore, can interact with the non-polar part of the ionomer backbone, enter the interstitial spaces of the crystalline phase, and soften them.

According to the Bloembergen–Purcell–Pound model, for long correlation times like in solids or polymers, a decrease in T_1 also indicates an increase in mobility. Therefore, an increase in mobility regarding all functional groups is generated by the hydration and separation of the pristine PEM. Concerning the samples under study, it is known from the literature that the hydrophilic percolation network of PFSA-ionomer membranes only forms in a humid state [65, 66]. Furthermore, a swelling of the membrane by 16% at a water mass fraction of 25% is reported, which suggests molecular motions to be less restricted [67].

The diffusion coefficients of the HS-PEM, the HS-MEA and the HHS-MEA confirm the significantly increased water uptake behaviour compared with the diffusion coefficient of the HP-PEM. The structure of the hydrated ionomer, as suggested by the significant decrease in ^{19}F T_1 after separation, gives rise to additional diffusion pathways and an increase in water-channel size. On the HP-PEM, a single exponential behaviour of the diffusion coefficient was observed, which indicates a fast exchange

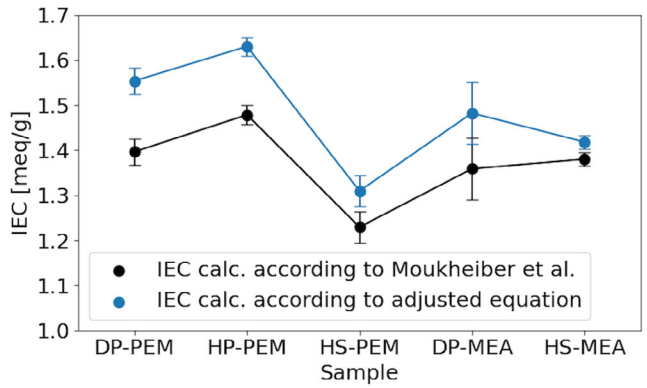

FIGURE 7 | Ionic exchange capacity (IEC) values calculated according to Moukheiber et al. [44] (black markers) and according to the adjusted Equation (11) (blue markers).

between surface and bulk diffusion inside the channels. After the separation, on the HS-PEM, HS-MEA and HHS-MEA, a double exponential behaviour was observed, attributing a slow exchange between both diffusion domains. Performing T_2-T_2 exchange experiments, Andrada et al. have found that proton exchange between the mobile and the slower diffusing water population in lsc-PFSA ionomer membranes no longer takes place at a relative humidity of more than 70% [55]. The higher diffusion coefficient was in the order of 10^{-9} m^2 s^{-1}, which reaches almost the diffusion coefficient of bulk water with 2.3×10^{-9} m^2 s^{-1} [68]. It should be noted that the Grotthuss mechanism cannot be resolved by NMR spectroscopy. Therefore, the proton conductivity determined by electrical impedance spectroscopy is reported as about double as high as the proton diffusion coefficient determined by PFG NMR, especially at a high water uptake ratio of 10 water molecules per sulfonic acid group [54]. It is therefore reasonable to assign the higher diffusion coefficient to the vehicle mechanism or, more generally, to the diffusion of free water in the centre of the channels. The lower diffusion coefficient, on the other hand, is attributed to the protons mainly transported by the hopping mechanism between the sulfonic acid groups. As the high T_2 on the HS-PEM, HS-MEA and HHS-MEA are attributed to high proton mobility, which refers to proton diffusion inside the bulk of the hydrophilic percolation network, the selectivity of the membrane, which is given by the sulfonic acid groups, must be questioned at this point.

In literature about PEM degradation, the ion exchange capacity is often discussed as a useful performance indicator of proton exchange membranes [43–45]. Here, the ion exchange capacity determination can serve as an estimate of how proton conduction is performed inside the membrane. In contrast to determining the proton diffusion coefficient by pulsed field gradient NMR techniques, the ion exchange capacity is calculated exclusively based on the ratio of the OCF_2 signal to the $(CF_2)_n$ signal, which represents the side chain and thus the part of the ionomer, to the molar mass of the ionomer.

The resulting ion exchange capacity calculated according to the model by Moukheiber et al. for each sample is represented by the black markers in Figure 7. These values are in the same order of magnitude as literature values determined for ssc-PFSA ionomers with several analysis methods, including NMR spectroscopy [44].

The separation process on the HS-PEM leads to a significant decrease in the IEC compared with the DP-PEM and HP-PEM. This can be explained by degradation by side-chain cleavage. However, the ion exchange capacity of the HS-MEA, where the separation process has also been performed, increases slightly in comparison to the DP-MEA.

The molar mass of the side chain with 278 g mol^{-1} in the calculation of Moukheiber et al. [44] results from the fact that only one of the CF_2 groups located directly next to the branching point is viewed as part of the side chain. In a later adjustment of this calculation, both CF_2 groups next to the branching point are viewed as part of the side chain, which results in a molar mass of $M_{ssc} = 328$ g mol^{-1}.

It is crucial to note that the SCF_2/CCF_2 signal contributes to the calculation as part of the backbone. However, derived from the molecular structure, the SCF_2/CCF_2 signal contributes partially to both the backbone with the two CCF_2 groups and the side chain with the SCF_2 group, as suggested by Schmidt-Rohr [69]. Thus, the model was adjusted to take into consideration that the SCF_2/CCF_2 signal contributes to the side chain. For that reason, the contribution of the SCF_2/CCF_2 signal to the denominator of the ratio is being eliminated (Equation 11):

$$R = \frac{I_{OCF_2}}{I_{(CF_2)_n}}. \tag{11}$$

By the applied fitting model presented in Figure 3A–E, a distinction between the $(CF_2)_n$ and the SCF_2/CCF_2 signal was possible. The blue markers in Figure 8 represent the adjusted ion exchange capacities according to the adjusted model. While the overall trend for the PEM samples and the DP-MEA remains unchanged, a slight decrease in the IEC of the HS-MEA is noticeable. However, the applied model is still questionable because it is not known whether the CCF_2 groups and the SCF_2 group are degraded to the same extent. Nevertheless, the data from the IEC evaluation can be regarded as a supplement to the results of the ^1H diffusion: While proton diffusion can be regarded as a general measure of mobility of mobile particles within the membrane, the ion exchange capacity includes the selectivity regarding the separation of cations and anions, which is defined by the available sulphonic acid groups. It can therefore be concluded that although the mobility within the membrane increases significantly by the separation process, the selectivity of the membrane for the transport of protons decreases. In the case of PFSA ionomers, the IEC can only be considered as an indicator of the selectivity of a PFSA membrane regarding proton transport, but not as a measure of the transport performance of a PFSA membrane.

5 | Conclusion

In this work, different NMR methods were employed that revealed significant structural and morphological differences between a pristine and a recycled PEM. The high significance of the NMR parameters, which are therefore suitable for evaluating recycling methods, is well demonstrated in this study.

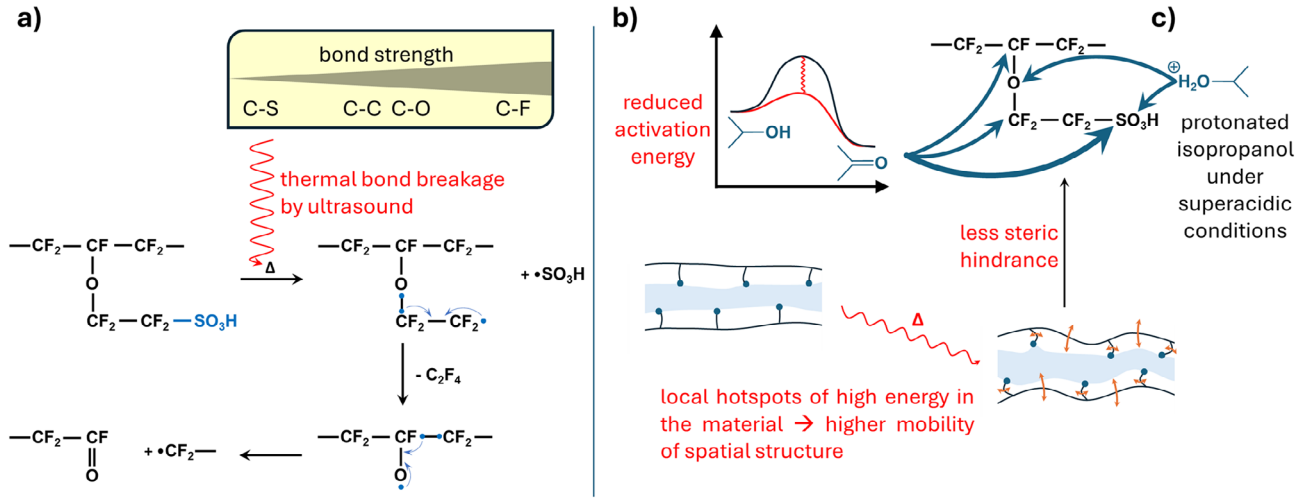

FIGURE 8 | Depiction of the different chemical degradation mechanisms occurring during the separation process that are discussed in this work, as suggested by the data. Red text and figure elements mark the influence of the ultrasound. The degradation mechanism, where thermal bond breakage by ultrasound is followed by radical chain unzipping, is displayed in (**a**). The reduction of the activation energy of the oxidation of isopropanol to acetone and the enhancement of the mobility of the ionomer structure, followed by nucleophilic attack reactions, is shown in (**b**). In (**c**), the electrophilic attack of isopropanol, which is protonated under superacidic conditions, is demonstrated.

By the analysis of the relative signal intensities of the side chain-related signals, it was found that the separation mechanism leads to a non-negligible degradation of sulfonic acid groups and complete side chains. A mechanism was proposed in which the degradation of the sulfonic acid groups is strongly linked to the degradation of complete side chains (Figure 8a). The use of ultrasonication is considered the main reason for degradation on a molecular level, as thermal breakage of the C–S bond could be induced by it. In addition, the ultrasound is considered to reduce the activation energy of the oxidation of isopropanol to acetone and, at the same time, to enhance the mobility of the molecular structure. The combination of these two effects could lead to nucleophilic attacks of the acetone at different sites of the PEM structure. Therefore, it could be an option to dispense with ultrasound for mechanical separation, thus preventing thermally induced bond breaks and the oxidation of the isopropanol. Another possible influence is the superacidic conditions inside the PEM, which could lead to side-chain scission in combination with the use of isopropanol (Figure 8c).

The study of sample relaxation behaviour and diffusivity revealed an increase in the mobility of ssc-PFSA functional groups depending on humidity, and particularly the separation process utilising isopropanol. In addition to increased proton diffusivity, the separation process led to the formation of two non-exchanging water domains representing different proton transportation modes, which cannot be attributed to an increased availability of sulfonic acid groups based on the IEC calculation. Instead, the increased proton mobility might be attributed to a higher fraction of free water due to a widening of the water-bearing channels. The increased proton mobility appears to be related to the use of isopropanol. Therefore, it is suggested to replace or use a smaller amount of isopropanol to avoid morphological changes influencing the proton selectivity of the membrane.

Overall, the NMR results obtained from high-field as well as low-field NMR devices suggest that the separation mechanism has a significant impact on the PEM. Therefore, this technique might not be suitable if recycling of the PFSA material is desired. This finding could be achieved by the analysis of ^{19}F signal ratios and the changes in T_1 relaxation behaviour. Nevertheless, the results of the ^{1}H methods provide correlated information. Since the 80 MHz benchtop NMR spectrometer is sufficient for these methods, it provides a less expensive and less complex alternative method compared with the ^{19}F MAS-NMR methods for screening PEM materials. The ^{19}F MAS-NMR methods, however, reveal additional details on PEM structure. Thus, samples identified as particularly promising by ^{1}H NMR methods can afterwards be examined in detail by ^{19}F NMR high-resolution techniques.

Author Contributions

Robert Rameker: investigation, formal analysis, data curation, validation, visualisation, software, writing – original draft. **Sven Jovanovic:** data curation, formal analysis, conceptualisation, software, writing – original draft. **Maik Plüm:** resources, conceptualisation, writing – review and editing. **Günter Schmid:** resources, supervision, writing – review and editing, funding acquisition. **André Karl:** supervision, project administration. **Eva Jodat:** supervision, project administration. **Rüdiger-A. Eichel:** supervision, writing – review and editing, project administration, funding acquisition. **Josef Granwehr:** formal analysis, supervision, writing – review and editing

Acknowledgements

The authors gratefully acknowledge the financial support by the German Federal Ministry of Education and Research (BMBF) within the H2Giga project DERIEL (grant number 03HY122C). Moreover, we would like to express our gratitude to Senem Ak and Chuan Qin, who provided significant assistance with sample preparation as part of their master's thesis at Siemens Energy. In addition, we gratefully acknowledge Peter Philipp Maria Schleker (Jülich Research Centre, IET-1) for his insightful scientific contributions to the discussion of our results.

Open access funding enabled and organized by Projekt DEAL.

Funding

This work was supported by the German Federal Ministry of Education and Research (BMBF) within the H2Giga project DERIEL (grant number 03HY122C).

Conflicts of Interest

The authors declare no conflicts of interest.

Data Availability Statement

The data are available for download on JülichDATA under the following link: https://doi.org/10.26165/JUELICH-DATA/O1U97K.

References

1. T. Banerjee, F. Podjaski, J. Kröger, B. P. Biswal, and B. V. Lotsch, "Polymer Photocatalysts for Solar-to-Chemical Energy Conversion," *Nature Reviews Materials* 6 (2021): 168–190, https://doi.org/10.1038/s41578-020-00254-z.

2. A. S. Aricò, S. Siracusano, N. Briguglio, V. Baglio, A. Di Blasi, and V. Antonucci, "Polymer Electrolyte Membrane Water Electrolysis: Status of Technologies and Potential Applications in Combination With Renewable Power Sources," *Journal of Applied Electrochemistry* 43 (2013): 107–118.

3. A. J. Botz, M. Nebel, R. A. Rincón, E. Ventosa, and W. Schuhmann, "Onset Potential Determination at Gas-Evolving Catalysts by Means of Constant-Distance Mode Positioning of Nanoelectrodes," *Electrochimica Acta* 179 (2015): 38–44, https://doi.org/10.1016/j.electacta.2015.04.145.

4. S. H. Frensch, F. Fouda-Onana, G. Serre, D. Thoby, S. S. Araya, and S. K. Kær, "Influence of the Operation Mode on PEM Water Electrolysis Degradation," *International Journal of Hydrogen Energy* 44 (2019): 29889–29898, https://doi.org/10.1016/j.ijhydene.2019.09.169.

5. M. Genovese, A. Schlüter, E. Scionti, F. Piraino, O. Corigliano, and P. Fragiacomo, "Power-to-Hydrogen and Hydrogen-to-X Energy Systems for the Industry of the Future in Europe," *International Journal of Hydrogen Energy* (2023): 16545–16568, https://doi.org/10.1016/j.ijhydene.2023.01.194.

6. M. Schalenbach, M. Carmo, D. L. Fritz, J. Mergel, and D. Stolten, "Pressurized PEM Water Electrolysis: Efficiency and Gas Crossover," *International Journal of Hydrogen Energy* 38 (2013): 14921–14933, https://doi.org/10.1016/j.ijhydene.2013.09.013.

7. *Hydrogen Production by Water Electrolysis: A Review of Alkaline Water Electrolysis, PEM Water Electrolysis and High Temperature Water Electrolysis*, 2015, https://www.researchgate.net/profile/hamid-naseem/publication/273125977_hydrogen_production_by_water_electrolysis_a_review_of_alkaline_water_electrolysis_pem_water_electrolysis_and_high_temperature_water_electrolysis.

8. Z. Ziobrowski and A. Rotkegel, "Assessment of Hydrogen Energy Industry Chain Based on Hydrogen Production Methods, Storage, and Utilization," *Energies* 17 (2024): 1808, https://doi.org/10.3390/en17081808.

9. M. Carmo, D. L. Fritz, J. Mergel, and D. Stolten, "A Comprehensive Review on PEM Water Electrolysis," *International Journal of Hydrogen Energy* 38 (2013): 4901–4934, https://doi.org/10.1016/j.ijhydene.2013.01.151.

10. C. Spöri, J. T. H. Kwan, A. Bonakdarpour, D. P. Wilkinson, and P. Strasser, "The Stability Challenges of Oxygen Evolving Catalysts: Towards a Common Fundamental Understanding and Mitigation of Catalyst Degradation," *Angewandte Chemie International Edition* 56 (2017): 5994–6021.

11. C. Gilliam and S. Kelleher, "Top US Chemical Firms to Pay $1.2bn to Settle Water Contamination Lawsuits. Dupont, Chemours and Corteva agree Deal and 3M Also Reportedly Considering $10bn Settlement to Avoid Trial Due to Start on Monday," (2023), *The Guardian*, 02.06.

12. C. Mindock, "3M, DuPont Defeat Massive Class Action Over Forever Chemicals," *Reuters* (2023), 28.11.

13. European Environment Agency. Was sind PFAS und inwiefern sind sie für meine Gesundheit gefährlich? (2023).

14. The PFAS Health Study: Systematic Literature Review, 2018, https://nceph.anu.edu.au/sites/prod.nceph.sca-lws06.anu.edu.au/files/pfas%20health%20study%20systematic%20review_1.pdf.

15. European Commission: Joint Research Centre, F. Neuwahl, M. Wegener, R. Salvucci, et al. *Clean Energy Technology Observatory: POTEnCIA CETO 2024 Scenario - 2024 Energy System Modelling for Clean Energy Technology Scenarios* Publications Office of the European Union, Luxembourg, 2024, https://data.europa.eu/doi/10.2760/1473321, JRC139836.

16. L. Gaines, "Lithium-ion Battery Recycling Processes: Research Towards a Sustainable Course," *Sustainable Materials and Technologies* 17 (2018): e00068, https://doi.org/10.1016/j.susmat.2018.e00068.

17. D. L. Thompson, J. M. Hartley, S. M. Lambert, et al., "The Importance of Design in Lithium Ion Battery Recycling—a Critical Review," *Green Chemistry* 22 (2020): 7585–7603, https://doi.org/10.1039/D0GC02745F.

18. P. Phogat, S. Dey, and M. Wan, "Powering the Sustainable Future: A Review of Emerging Battery Technologies and Their Environmental Impact," *RSC Sustainability* (2025): 3266–3306, https://doi.org/10.1039/D5SU00127G.

19. B. K. Biswal, B. Zhang, P. Thi Minh Tran, J. Zhang, and R. Balasubramanian, "Recycling of Spent Lithium-Ion Batteries for a Sustainable Future: Recent Advancements," *Chemical Society Reviews* 53 (2024): 5552–5592, https://doi.org/10.1039/D3CS00898C.

20. E. Dinneya-Onuoha, "Unlocking Renewable Energy Materials in Nigeria: Availability, Application, and Roadmap for Sustainability," *RSC Sustainability* 3 (2025): 2534–2566, https://doi.org/10.1039/D5SU00121H.

21. Z. Wu, M. Sytnyk, J. Zhang, et al., "Closing the Loop: Recycling of MAPbI 3 Perovskite Solar Cells," *Energy & Environmental Science* 17 (2024): 4248–4262, https://doi.org/10.1039/D4EE01071J.

22. M. E. Keal, S. Scott, N. N. Alsulami, et al., "Design for Recycle of Devices to Ensure Efficient Recovery of Technology Critical Metals," *RSC Sustainability* 3 (2025): 2455–2471, https://doi.org/10.1039/D5SU00128E.

23. X. Luo, S. Holdcroft, A. Mani, Y. Zhang, and Z. Shi, "Water, Proton, and Oxygen Transport in High IEC, Short Side Chain PFSA Ionomer Membranes: Consequences of a Frustrated Network," *Physical Chemistry Chemical Physics* 13 (2011): 18055, https://doi.org/10.1039/c1cp22559f.

24. K. D. Kreuer, M. Schuster, B. Obliers, et al., "Short-side-chain Proton Conducting Perfluorosulfonic Acid Ionomers: Why They Perform Better in PEM Fuel Cells," *Journal of Power Sources* 178 (2008): 499–509, https://doi.org/10.1016/j.jpowsour.2007.11.011.

25. F. Fouda-Onana, M. Chandesris, V. Médeau, S. Chelghoum, D. Thoby, and N. Guillet, "Investigation on the Degradation of MEAs for PEM Water Electrolysers Part I: Effects of Testing Conditions on MEA Performances and Membrane Properties," *International Journal of Hydrogen Energy* 41 (2016): 16627–16636, https://doi.org/10.1016/j.ijhydene.2016.07.125.

26. N. Li, S. S. Araya, and S. K. Kær, "Long-Term Contamination Effect of Iron Ions on Cell Performance Degradation of Proton Exchange Membrane Water Electrolyser," *Journal of Power Sources* 434 (2019): 226755, https://doi.org/10.1016/j.jpowsour.2019.226755.

27. E. Padgett, A. Adesso, H. Yu, et al., "Performance Losses and Current-Driven Recovery From Cation Contaminants in PEM Water Electrolysis," *Journal of the Electrochemical Society* 171 (2024): 064510, https://doi.org/10.1149/1945-7111/ad576b.

28. X. Wang, L. Zhang, G. Li, G. Zhang, Z.-G. Shao, and B. Yi, "The Influence of Ferric Ion Contamination on the Solid Polymer Electrolyte Water Electrolysis Performance," *Electrochimica Acta* 158 (2015): 253–257, https://doi.org/10.1016/j.electacta.2015.01.140.

29. V. O. Mittal, H. R. Kunz, and J. M. Fenton, "Membrane Degradation Mechanisms in PEMFCs," *Journal of the Electrochemical Society* 154 (2007): B652, https://doi.org/10.1149/1.2734869.

30. H. Tang, M. Pan, F. Wang, P. K. Shen, and S. P. Jiang, "Highly Durable Proton Exchange Membranes for Low Temperature Fuel Cells," *The Journal of Physical Chemistry B* 111 (2007): 8684–8690, https://doi.org/10.1021/jp073136t.

31. P. Marocco, K. Sundseth, T. Aarhaug, et al., "Online Measurements of Fluoride Ions in Proton Exchange Membrane Water Electrolysis Through Ion Chromatography," *Journal of Power Sources* 483 (2021): 229179, https://doi.org/10.1016/j.jpowsour.2020.229179.

32. L. Ghassemzadeh, K.-D. Kreuer, J. Maier, and K. Müller, "Chemical Degradation of Nafion Membranes Under Mimic Fuel Cell Conditions as Investigated by Solid-State NMR Spectroscopy," *Journal of Physical Chemistry C* 114 (2010): 14635–14645, https://doi.org/10.1021/jp102533v.

33. J. Healy, C. Hayden, T. Xie, et al., "Aspects of the Chemical Degradation of PFSA Ionomers Used in PEM Fuel Cells," *Fuel Cells* 5 (2005): 302–308, https://doi.org/10.1002/fuce.200400050.

34. M. Chandesris, V. Médeau, N. Guillet, S. Chelghoum, D. Thoby, and F. Fouda-Onana, "Membrane Degradation in PEM Water Electrolyzer: Numerical Modeling and Experimental Evidence of the Influence of Temperature and Current Density," *International Journal of Hydrogen Energy* 40 (2015): 1353–1366, https://doi.org/10.1016/j.ijhydene.2014.11.111.

35. M. Carmo, G. P. Keeley, D. Holtz, et al., "PEM Water Electrolysis: Innovative Approaches Towards Catalyst Separation, Recovery and Recycling," *International Journal of Hydrogen Energy* 44 (2019): 3450–3455, https://doi.org/10.1016/j.ijhydene.2018.12.030.

36. C. Li, A. Sallee, X. Zhang, and S. Kumar, "Electrochemical Hydrogenation of Acetone to Produce Isopropanol Using a Polymer Electrolyte Membrane Reactor," *Energies* 11 (2018): 2691, https://doi.org/10.3390/en11102691.

37. L. Shore, (2006) Process for recycling components of a PEM fuel cell membrane electrode assembly. US Patent 8,124,261 B2, filed 20 June 2006 and published 28 february 2012.

38. J. Alipour Moghaddam, M. J. Parnian, and S. Rowshanzamir, "Preparation, Characterization, and Electrochemical Properties Investigation of Recycled Proton Exchange Membrane for Fuel Cell Applications," *Energy* 161 (2018): 699–709, https://doi.org/10.1016/j.energy.2018.07.123.

39. Z. J. Baum, R. E. Bird, X. Yu, and J. Ma, "Lithium-Ion Battery Recycling—Overview of Techniques and Trends," *ACS Energy Letter* 7 (2022): 712–719, https://doi.org/10.1021/acsenergylett.1c02602.

40. M. Rezaei, A. Nekahi, A. Kumar M R, et al., "A Review of Lithium-Ion Battery Recycling for Enabling a Circular Economy," *Journal of Power Sources* 630 (2025): 236157, https://doi.org/10.1016/j.jpowsour.2024.236157.

41. T. Yingnakorn, J. Hartley, M. E. Keal, et al., "Catalyst Coated Membranes for Fuel Cell and Water Electrolyser Delamination Induced by Organic Solution Soaking and Water Ultrasonication," *RSC Sustainability* 3 (2025): 1900–1908, https://doi.org/10.1039/D4SU00795F.

42. L. Ghassemzadeh, K. D. Kreuer, J. Maier, and K. Müller, "Evaluating Chemical Degradation of Proton Conducting Perfluorosulfonic Acid Ionomers in a Fenton Test by Solid-state 19F NMR Spectroscopy," *Journal of Power Sources* 196 (2011): 2490–2497, https://doi.org/10.1016/j.jpowsour.2010.11.053.

43. L. Ghassemzadeh and S. Holdcroft, "Quantifying the Structural Changes of Perfluorosulfonated Acid Ionomer Upon Reaction With Hydroxyl Radicals," *Journal of the American Chemical Society* 135 (2013): 8181–8184, https://doi.org/10.1021/ja4037466.

44. E. Moukheiber, G. D. Moor, L. Flandin, and C. Bas, "Investigation of Ionomer Structure Through Its Dependence on Ion Exchange Capacity (IEC)," *Journal of Membrane Science* 389 (2012): 294–304, https://doi.org/10.1016/j.memsci.2011.10.041.

45. M. Robert, A. E. Kaddouri, J.-C. Perrin, S. Leclerc, and O. Lottin, "Towards a NMR-Based Method for Characterizing the Degradation of Nafion XL Membranes for PEMFC," *Journal of the Electrochemical Society* 165 (2018): F3209–F3216, https://doi.org/10.1149/2.0231806jes.

46. L. Ghassemzadeh, M. Marrony, R. Barrera, K. D. Kreuer, J. Maier, and K. Müller, "Chemical Degradation of Proton Conducting Perfluorosulfonic Acid Ionomer Membranes Studied by Solid-State Nuclear Magnetic Resonance Spectroscopy," *Journal of Power Sources* 186 (2009): 334–338, https://doi.org/10.1016/j.jpowsour.2008.10.004.

47. C. Lim, L. Ghassemzadeh, F. van Hove, et al., "Membrane Degradation During Combined Chemical and Mechanical Accelerated Stress Testing of Polymer Electrolyte Fuel Cells," *Journal of Power Sources* 257 (2014): 102–110, https://doi.org/10.1016/j.jpowsour.2014.01.106.

48. I. Nicotera, K. Angjeli, L. Coppola, et al., "Composite Polymer Electrolyte Membranes Based on Mg–Al Layered Double Hydroxide (LDH) Platelets for H2/Air-Fed Fuel Cells," *Solid State Ionics* 276 (2015): 40–46, https://doi.org/10.1016/j.ssi.2015.03.037.

49. Y. J. Jiang and J. K. Harper, "An Explanation of Magic Angle Spinning NMR Experiments in the Time Domain," *Concepts in Magnetic Resonance* 34A (2009): 249–263, https://doi.org/10.1002/cmr.a.20144.

50. D. D. Laws, H.-M. L. Bitter, and A. Jerschow, "Methoden der Festkrper-NMR-Spektroskopie in der Chemie," *Angewandte Chemie* 114 (2002): 3224–3259, https://doi.org/10.1002/1521-3757(20020902)114:17%3c3224::AID-ANGE3224%3e3.0.CO;2-C.

51. T. Zelovich, L. Vogt-Maranto, C. Simari, et al., "Non-Monotonic Temperature Dependence of Hydroxide Ion Diffusion in Anion Exchange Membranes," *Chemistry of Materials* 34 (2022): 2133–2145, https://doi.org/10.1021/acs.chemmater.1c03594.

52. D. K. Lee, T. Saito, A. J. Benesi, M. A. Hickner, and H. R. Allcock, "Characterization of Water in Proton-conducting Membranes by Deuterium NMR T1 Relaxation," *Journal of Physical Chemistry B* 115 (2011): 776–783, https://doi.org/10.1021/jp106757b.

53. I. Nicotera, V. Kosma, C. Simari, C. D'Urso, A. S. Aricò, and V. Baglio, "Methanol and Proton Transport in Layered Double Hydroxide and Smectite Clay-Based Composites: Influence on the Electrochemical Behavior of Direct Methanol Fuel Cells at Intermediate Temperatures," *Journal of Solid State Electrochemistry* 19 (2015): 2053–2061, https://doi.org/10.1007/s10008-014-2701-y.

54. S. Ochi, O. Kamishima, J. Mizusaki, and J. Kawamura, "Investigation of Proton Diffusion in Nafion®117 Membrane by Electrical Conductivity and NMR," *Solid State Ionics* 180 (2009): 580–584, https://doi.org/10.1016/j.ssi.2008.12.035.

55. H. E. Andrada, M. B. Franzoni, A. C. Carreras, and F. V. Chávez, "Dynamics and Spatial Distribution of Water in Nafion 117 Membrane Investigated by NMR Spin-Spin Relaxation," *International Journal of Hydrogen Energy* 43 (2018): 8936–8943, https://doi.org/10.1016/j.ijhydene.2018.03.124.

56. I. Nicotera, V. Kosma, C. Simari, et al., "An NMR Study on the Molecular Dynamic and Exchange Effects in Composite Nafion/Sulfated Titania Membranes for PEMFCs," *International Journal of Hydrogen Energy* 40 (2015): 14651–14660, https://doi.org/10.1016/j.ijhydene.2015.06.137.

57. M. Newville, T. Stensitzki, D. B. Allen, M. Rawlik, A. Ingargiola, and A. L. Nelson, "Non-Linear Least-Square Minimization and Curve-Fitting for Python," *Astrophysics Source Code Library* (2016), ascl:1606.014.

58. D. Sinnaeve, "The Stejskal–Tanner Equation Generalized for any Gradient Shape—An Overview of Most Pulse Sequences Measuring Free Diffusion," *Concepts Magnetic Resonance* 40A (2012): 39–65, https://doi.org/10.1002/cmr.a.21223.

59. C. A. Clark and D. Le Bihan, "Water Diffusion Compartmentation and Anisotropy at High b Values in the human Brain," *Magnetic Resonance in Medicine* 44 (2000): 852–859, https://doi.org/10.1002/1522-2594(200012)44:6%3c852::AID-MRM5%3e3.0.CO;2-A.

60. J. Hrabe, G. Kaur, and D. N. Guilfoyle, "Principles and Limitations of NMR Diffusion Measurements," *Journal of Medicine Physics* 32 (2007): 34, https://doi.org/10.4103/0971-6203.31148.

61. R. Hammer, M. Schönhoff, and M. R. Hansen, "Comprehensive Picture of Water Dynamics in Nafion Membranes at Different Levels of

Hydration," *Journal of Physical Chemistry B* 123 (2019): 8313–8324, https://doi.org/10.1021/acs.jpcb.9b05093.

62. S. You, M.-W. Chen, D. D. Dlott, and K. S. Suslick, "Ultrasonic Hammer Produces Hot Spots in Solids," *Nature Communications* 6 (2015): 6581, https://doi.org/10.1038/ncomms7581.

63. M. Xu, F. Xin, X. Li, X. Huai, and H. Liu, "Ultrasound Promoted Catalytic Liquid-Phase Dehydrogenation of Isopropanol for Isopropanol-Acetone-Hydrogen Chemical Heat Pump," *Ultrasonics Sonochemistry* 23 (2015): 66–74, https://doi.org/10.1016/j.ultsonch.2014.09.003.

64. J. M. J. Paulusse and R. P. Sijbesma, "Ultrasound in Polymer Chemistry: Revival of an Established Technique," *Journal of Polymer Science A Polymer Chemistry* 44 (2006): 5445–5453, https://doi.org/10.1002/pola.21646.

65. W. Gonçalves, T. Mabuchi, and T. Tokumasu, "Nucleation and Growth of Cavities in Hydrated Nafion Membranes Under Tensile Strain: A Molecular Dynamics Study," *Journal of Physical Chemistry C* 123 (2019): 28958–28968, https://doi.org/10.1021/acs.jpcc.9b07101.

66. L. Chaabane, L. Dammak, D. Grande, et al., "Swelling and Permeability of Nafion®117 in Water–Methanol Solutions: An Experimental and Modelling Investigation," *Journal of Membrane Science* 377 (2011): 54–64, https://doi.org/10.1016/j.memsci.2011.03.037.

67. E. H. Sanders, K. A. McGrady, G. E. Wnek, et al., "Characterization of Electrosprayed Nafion Films," *Journal of Power Sources* 129 (2004): 55–61, https://doi.org/10.1016/j.jpowsour.2003.11.020.

68. G. Dorenbos and Y. Suga, "Simulation of Equivalent Weight Dependence of Nafion Morphologies and Predicted Trends Regarding Water Diffusion," *Journal of Membrane Science* 330 (2009): 5–20, https://doi.org/10.1016/j.memsci.2008.11.056.

69. Q. Chen and K. Schmidt-Rohr, "19 F and 13 C NMR Signal Assignment and Analysis in a Perfluorinated Ionomer (Nafion) by Two-Dimensional Solid-State NMR," *Macromolecules* 37 (2004): 5995–6003, https://doi.org/10.1021/ma049759b.

Supporting Information

Additional supporting information can be found online in the Supporting Information section.

Supporting File: elsa70025-sup-0001-SuppMat.docx.